


## Tunable energy spectrum betatron x-ray sources in a plasma wakefield

Chuan-Yi Xi(奚传易), Yin-Ren Shou(寿寅任), Li-Qi Han(韩立琦), Abdughupur Ablimit(阿卜杜伍普尔·阿布力米提), Xiao-Dan Liu(刘晓丹), Yan-Ying Zhao(赵研英), and Jin-Qing Yu(余金清)
**Citation:**Chin. Phys. B, 2024, 33 (**8**): 085202. DOI: 10.1088/1674-1056/ad4531

**What follows is a list of articles you may be interested in**

---

## Electromagnetic pulses produced by a picosecond laser interacting with solid targets

Ai-Hui Niu(牛爱慧), Ning Kang(康宁), Guo-Xiao Xu(许国潇), Jia-Jie Xie(谢佳节), Jian Teng(滕建), Hui-Ya Liu(刘会亚), Ming-Ying Sun(孙明营), and Ting-Shuai Li(李廷帅)
Chin. Phys. B, 2024, 33 (**5**): 054205. DOI: 10.1088/1674-1056/ad1a95

## Effect of sharp vacuum-plasma boundary on the electron injection and acceleration in a few-cycle laser driven wakefield

Guo-Bo Zhang(张国博), Song Liu(刘松), De-Bin Zou(邹德滨), Ye Cui(崔野), Jian-Peng Liu(刘建鹏), Xiao-Hu Yang(杨晓虎), Yan-Yun Ma(马燕云), and Fu-Qiu Shao(邵福球)
Chin. Phys. B, 2023, 32 (**9**): 095202. DOI: 10.1088/1674-1056/acdc0c

## Electron acceleration during magnetic islands coalescence and division process in a guide field reconnection

Shengxing Han(韩圣星), Huanyu Wang(王焕宇), and Xinliang Gao(高新亮)
Chin. Phys. B, 2022, 31 (**2**): 025202. DOI: 10.1088/1674-1056/ac21c0

## Ultrabright $\gamma$-ray emission from the interaction of an intense laser pulse with a near-critical-density plasma

Aynisa Tursun(阿依妮萨·图尔苏), Mamat Ali Bake(买买提艾力·巴克), Baisong Xie(谢柏松), Yasheng Niyazi(亚生·尼亚孜), and Abuduresuli Abudurexiti(阿不都热苏力·阿不都热西提)
Chin. Phys. B, 2021, 30 (**11**): 115202. DOI: 10.1088/1674-1056/abfb59

## Acceleration and radiation of externally injected electrons in laser plasma wakefield driven by a Laguerre-Gaussian pulse

Zhong-Chen Shen(沈众辰), Min Chen(陈民), Guo-Bo Zhang(张国博), Ji Luo(罗辑), Su-Ming Weng(翁苏明), Xiao-Hui Yuan(远晓辉), Feng Liu(刘峰), Zheng-Ming Sheng(盛政明)
Chin. Phys. B, 2017, 26 (**11**): 115204. DOI: 10.1088/1674-1056/26/11/115204

---

# Tunable energy spectrum betatron x-ray sources in a plasma wakefield

Chuan-Yi Xi(奚传易)[1], Yin-Ren Shou(寿寅任)[2], Li-Qi Han(韩立琦)[1], Abdughupur Ablimit(阿卜杜伍普尔·阿布力米提)[1], Xiao-Dan Liu(刘晓丹)[1], Yan-Ying Zhao(赵研英)[3,†], and Jin-Qing Yu(余金清)[1]

[1] *Hunan Provincial Key Laboratory of High-Energy Scale Physics and Applications, School of Physics and Electronics, Hunan University, Changsha* 410082, *China*

[2] *Center for Relativistic Laser Science, Institute for Basic Science, Gwangju, Korea*

[3] *State Key Laboratory of Nuclear Physics and Technology, and Key Laboratory of HEDP of the Ministry of Education, CAPT, Peking University, Beijing* 100871, *China*

(Received 27 February 2024; revised manuscript received 23 April 2024; accepted manuscript online 30 April 2024)

X-ray sources with tunable energy spectra have a wide range of applications in different scenarios due to their different penetration depths. However, existing x-ray sources face difficulties in terms of energy regulation. In this paper, we present a scheme for tuning the energy spectrum of a betatron x-ray generated from a relativistic electron bunch oscillating in a plasma wakefield. The center energy of the x-ray source can be tuned from several keV to several hundred keV by changing the plasma density, thereby extending the control range by an order of magnitude. At different central energies, the brightness of the betatron radiation is in the range of $3.7\times10^{22}$ to $5.5\times10^{22}$ photons/(0.1%BW·s·mm$^2$·mrad$^2$) and the photon divergence angle is about 2 mrad. This high-brightness, energy-controlled betatron source could pave the way to a wide range of applications requiring photons of specific energy, such as phase-contrast imaging in medicine, non-destructive testing and material analysis in industry, and imaging in nuclear physics.

**Keywords:** betatron, plasma physics, x-ray, plasma wakefield acceleration (PWFA)

**PACS:** 52.38.Ph, 52.40.–w, 52.65.Rr **DOI:** 10.1088/1674-1056/ad4531

## 1. Introduction

Since x-rays were discovered, they have been widely used in biomedical, industrial, national defense and other fields. The usual means to obtain x-ray sources is to use traditional large accelerators, which are expensive and occupy a large area. The maximum acceleration gradient that can be achieved at present is 100 MV/m.[1,2] With the development of chirped pulse amplification (CPA) technology,[3] the intensity of lasers has significantly increased and the application of lasers has become more and more extensive, including the laser electron acceleration proposed by Tajima and Dawson in 1979.[4] The interaction between lasers and plasma has attracted more and more attention,[5] especially the radiation sources based on the laser-plasma wakefield, such as betatron radiation,[6] Compton scattering and free electron lasers. Betatron radiation sources use the electron beam generated by the interaction of a laser and plasma to oscillate the plasma and produce radiation.[7] Compared with traditional synchrotron radiation sources, betatron sources have the advantages of ultra-high brightness,[8] small source size,[9] ultra-short duration,[10] low divergence,[11] broad spectrum[12] and compactness.[13] These features collectively make betatron sources a promising and potentially significant advance in radiation source technology.[14]

Low-energy x-rays are widely used in routine biomedical imaging,[15] such as phase-contrast imaging and three-dimensional medical imaging of bones, while high-energy x-rays can penetrate thicker materials and are therefore widely applied in fields such as materials science,[16] physics[17] and chemistry.[18] Therefore, x-rays need to be flexibly tuned over a wide range of energies; however, both traditional synchrotron radiation sources and laser-plasma betatron radiation sources face several challenges in tuning x-ray energy.[19] The energy of the electron beam in traditional synchrotron radiation is controlled by the accelerator system, which requires modifications of the accelerator parameters, typically involving costly equipment and complex operations;[20] while adjustments to the electron's orbit radius in the storage ring are constrained by the magnetic field strength, requiring a complex magnetic field control system and affecting beam stability.[21] Tuning the photon spectrum in the laser-plasma betatron regime also presents challenges,[22] such as the readjustment of laser parameters and control of the injected electron charge.

In recent years, a number of research teams have been working on tuning x-ray energy.[23] The main achievement has been to obtain tunable x-ray sources in the range of tens of keV, with an emphasis on the oscillating electrons reaching energies in the range of 50 MeV to 250 MeV. As a result, the photons obtained are tunable within the range of tens

†Corresponding author. E-mail: zhaoyanying@pku.edu.cn

© 2024 Chinese Physical Society and IOP Publishing Ltd 

of keV.[24] Researchers from Peking University have studied the characteristics of betatron radiation in direct laser acceleration, and by changing the $a_0$ of the drive laser, they have been able to control the number and energy of radiation photons and achieve controllable central energies within a few keV.[25] Another research group has also observed fluctuations in the central energy and number of radiation photons when altering plasma density.[26] It can be found that, in previous studies of energy spectrum control, there are many methods for changing the injected electron energy or laser parameter $a_0$ to alter the energy of the accelerated electrons, thereby affecting the radiation spectrum. However, these methods not only exhibit poor experimental controllability but also have a limited tuning range, typically not exceeding one order of magnitude. Therefore, there is an urgent need for new technologies to obtain tunable x-ray sources with adjustable spectra.[27,28]

Beam-driven wakefield acceleration has the potential to overcome the limitations of traditional synchrotron radiation sources in adjusting x-ray energy.[29] By changing plasma density and adjusting beam-matching conditions, plasma wakefield acceleration can provide a method to accurately control the energy of accelerating electrons,[30] which in turn enables the generation of x-rays with tunable energy spectra. The development and implementation of plasma wakefield acceleration technology present a compelling opportunity to advance the field of x-ray science and enable new capabilities.[22]

In this paper, according to the existing scheme[31] to separate the electron acceleration process from the radiation process, we can ensure that the high-quality radiation of the electron beam and the radiation will be more controllable. Our primary focus was on the discussion of the effects of plasma on beam-focusing optimization. Subsequently, we determined the matching parameters of the beam and plasma and increased the number of oscillation periods while ensuring the betatron amplitude in order to enhance the x-ray brightness. Finally, an x-ray source with a tunable center energy from 1.4 keV to 102.1 keV was achieved by adjusting the plasma density to alter the beam oscillation frequency, while the brightness remained $3.7\times10^{22}$ to $5.5\times10^{22}$ photons/(0.1%BW·s·mm$^2$·mrad$^2$), and the full width at half maximum (FWHM) of the spot size was kept between 2.8 μm and 5.6 μm, which is smaller than the laser wakefield acceleration (LWFA)-based betatron x-ray spot size. In LWFA, to obtain the betatron x-ray with large energy, the x-ray spot often reaches tens of microns.[32] This tunable x-ray source shows promising potential for diverse applications in scientific research and industrial processes.

This paper is organized as follows. In Section 2, we investigate the betatron radiation spectrum in the interaction of beam-driven plasma based on existing theoretical research. In Section 3, we discuss the simulation results of beam-driven betatron radiation. In Section 4, we conclude this work.

## 2. Principles of the betatron radiation spectrum elucidated through beam-plasma interactions

In the bubble acceleration regime, the plasma cavity can act as a wiggler in addition to being an accelerator, reproducing synchrotron x-rays.[29] The bubble regime is reached when an intense electron beam, propagating in an underdense plasma, evacuates plasma electrons from the high-intensity regions and leaves an ion cavity. The sphericity of the ion cavity results in a transverse electric field, creating a restoring force along the direction of beam propagation.[33] As the electrons oscillate transversely in the cavity, satisfying the necessary conditions for producing accelerated charged particle radiation, the collimating radiation emitted by this electron beam is known as betatron radiation.[34]

Inside the ion cavity,[35,36] the electromagnetic fields consist of an axial electric field $E_z$, a radial electric field $E_r$ and an azimuthal magnetic field $B_\theta$, which are given by $E_z/E_0{=}k_{\rm p}\zeta/2$, $E_r/E_0 = k_{\rm p}r/4$, $B_\theta/E_0 = -k_{\rm p}r/(4c)$, where $\zeta = z - vt$ is the comoving variable, $\omega_{\rm p} = \sqrt{n_{\rm e}e^2/(m\varepsilon_0)}$ is the plasma frequency and $E_0 = m\omega_{\rm p}c/e$ is the cold non-relativistic wave-breaking field.[37] The cavity structures play a role similar to that of the undulator or wiggler in traditional radiation sources. When relativistic electrons propagate in the cavity, the equation of motion of electrons can be obtained as[38]

$$\frac{{\rm d}\boldsymbol{p}}{{\rm d}t} = -e(\boldsymbol{E}+\boldsymbol{v}\times\boldsymbol{B}) = \boldsymbol{F}_{\parallel}+\boldsymbol{F}_{\perp} \cong -\frac{m\omega_{\rm p}^2(\zeta\boldsymbol{e}_z + r\boldsymbol{e}_r)}{2}. \quad (1)$$

Therefore, the electron beam inside the cavity is subject to both a longitudinal accelerating field and a transverse focusing field.[6] Two crucial parameters for this process are the wavelength of the betatron motion $\lambda_\beta$[39] and the radiation intensity parameter $K$. In practical units, the two expressions read[42]

$$\lambda_\beta[\mu{\rm m}] = 4.72\times10^{10}\sqrt{\gamma/n_{\rm e}[{\rm cm}^{-3}]}, \quad (2)$$

$$K = 1.33\times10^{-10}\sqrt{\gamma n_{\rm e}[{\rm cm}^{-3}]}\,r_\beta[\mu{\rm m}], \quad (3)$$

where $\gamma(t)$ is the electron relativistic factor and $r_\beta$ is the electron oscillation amplitude.

Since the betatron oscillation wavelength is much shorter than in the wigglers case, when the relativistic factor $\gamma > 200$ or the energy is greater than 100 MeV, the emitted radiation falls within the x-ray range.[12] In the case of different $K$ values, the radiation spectrum is narrow or harmonic. The radiation spectrum decays exponentially, with a radiation angle $\theta = K/\gamma$. Its spectral distribution is a wide-spectrum structure, which can be expressed as[40]

$$\frac{{\rm d}^2I}{{\rm d}E\,{\rm d}\Omega} \sim N_\beta\frac{3e^2}{2\pi^3\hbar c\varepsilon_0}\gamma^2(E/E_{\rm c})^2\cdot K_{2/3}^2(E/E_{\rm c}), \quad (4)$$

where $I$ is the radiation energy, $N_\beta$ is the number of oscillating electrons, $K_{2/3}$ is the modified Bessel function and $E_c = 3/2K\gamma^2\hbar\omega_\beta$ is the critical energy. For a small amplitude of betatron oscillation $K \ll 1$, the radiation is emitted at the fundamental photon energy $\hbar\omega$ with a narrow bandwidth in the forward direction ($\theta = 0$). As $K$ approaches 1, harmonics of the fundamental start to appear in the spectrum. For $K \gg 1$, the spectrum contains many closely spaced harmonics and extends up to a critical energy $\hbar\omega_c$. These cases are given by[32]

$$\hbar\omega[\mathrm{eV}] = 5.25\times10^{-11}\gamma^{1.5}\sqrt{n_e[\mathrm{cm}^{-3}]} \quad \text{for } K \ll 1, \tag{5}$$

$$\hbar\omega_c[\mathrm{eV}] = 5.24\times10^{-21}\gamma^2 n_e[\mathrm{cm}^{-3}]\gamma_\beta[\mu\mathrm{m}] \quad \text{for } K \gg 1. \tag{6}$$

According to the aforementioned theory, to increase radiation energy, it is necessary to modify the frequency of radiation oscillations, rather than just changing the energy of the injected electron beam.

In Eq. (1), the term $\boldsymbol{F}_\parallel$ is responsible for the electron acceleration in the longitudinal direction. As the electron becomes relativistic, its velocity becomes higher than the group velocity of the wake,[41] the term $-\zeta$ decreases and the accelerating force is reduced. The distance for the electron to reach the middle of the cavity ($\zeta = 0$) and to become decelerated ($\zeta > 0$) corresponds to the dephasing length. The term $\boldsymbol{F}_\perp$ is a linear restoring force that drives the transverse oscillations of the electron across the cavity axis at the betatron frequency $\omega_\beta = \omega_p/\sqrt{2\gamma}$. Therefore, we should increase the transverse field as much as possible when the longitudinal accelerating field is stable so as to increase the electron beam oscillation, thereby enhancing electron oscillations and resulting in stronger electron radiation.

## 3. Simulation of beam driven betatron oscillation

In strong nonlinear cases, numerical simulations are necessary to obtain the actual wakefield. Separating the beam acceleration process from the oscillation process allows for the utilization of beams obtained from LWFA or traditional accelerators to achieve betatron radiation through the transverse focusing effect of the plasma wakefield acceleration (PWFA), which aims to accelerate charged particles using electromagnetic wave wakefields in plasma, and it has the advantage of greatly enhancing the collimation of the radiation.[42] Therefore, in our simulations, we use beam parameters already available from LWFA experiments[43] to exclusively simulate the x-ray generation through betatron oscillations in the PWFA process.

Since our simulation requires frequent calculations of radiation spectrum information, we verified the scheme using 3D PIC code EPOCH3D, which can treat the photons as particles. We could then obtain the corresponding information for each macro-photon.[44] In our settings, the drive beam propagates in the $x$-direction along a fully ionized plasma, the peak density of the drive beam $n_b$ is four times greater than the plasma density $n_e$. We used a moving window with a simulation window size of 100 μm×40 μm×40 μm and an open boundary, which was divided into $300\times120\times120$ cells with eight electrons per cell.[45] The simulated 3D betatron setup is shown in Fig. 1, which shows the PWFA process in which the front section of the beam drives the plasma wakefield to form a bubble structure and the back section of the beam oscillates under the action of the transverse field to generate betatron x-rays. The drive beam has a Gaussian transverse profile and a uniform longitudinal profile, with an energy spread (RMS) of about 10%. The plasma density $n_e$ was between $1\times10^{17}$ cm$^{-3}$ and $1\times10^{19}$ cm$^{-3}$. Chirped beams cause a series of adverse effects such as instability and decrease of electron acceleration efficiency. Therefore, in order to form a stable cavity and avoid beam emittance growth, the drive beam should be uniform or satisfy the Gaussian distribution and the size of the drive beam should match the plasma parameters. According to the existing theory,[46,47] the matched radial beam parameter for a Gaussian beam in the plasma ion column is defined by[48]

$$\sigma_r = \left(\frac{2\varepsilon_b^2}{\gamma_0 k_p^2}\right)^{1/4}, \tag{7}$$

where $\varepsilon_b$ is the normalized RMS emittance, and $\gamma_0$ is the initial mean Lorentz factor of the beam.

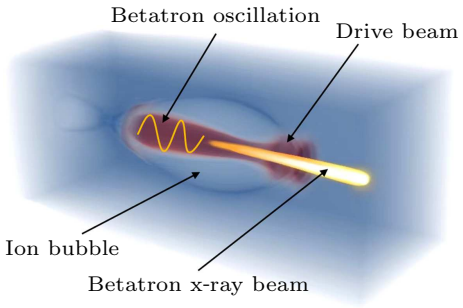



**Fig. 1.** Schematics for the setup of betatron radiation driven by an electron beam of 1.2 GeV. When the drive beam (red) propagates in the plasma, the space charge force pushes the electrons in the plasma, forming a bubble. Within the bubble, no additional injection of electrons is required. The electrons at the tail of the drive beam oscillate under the action of the transverse focusing field, generating betatron radiation (yellow) as they move forward.

Based on the theoretical model mentioned above[49] and the available experimental data,[22,50,51] the radial size $k_p\sigma_r = 0.6$ of the beam is beneficial for the generation of wakefield theoretically and can be realized experimentally.

Next, we determine the longitudinal dimensions of the beam.[52] During the beam-driven process, the beam and plasma modulate each other. Our approach employs the non-laser beam center-of-mass equation,[14] which under the adia-

batic approximation satisfies the following equation:[53]

$$\frac{\mathrm{d}\boldsymbol{p}_\perp}{\mathrm{d}t} = \frac{\mathrm{d}}{\mathrm{d}t}\left(\gamma\frac{\mathrm{d}\boldsymbol{r}}{\mathrm{d}t}\right) = -(\boldsymbol{E}_r - \boldsymbol{V}_x \times \boldsymbol{B}_\theta). \tag{8}$$

Under the adiabatic approximation, with the $X$-axis as the beam propagation direction, when the geometric center of the beam $x_\mathrm{c}$ is shifted by centroid $x_\mathrm{b}$,

$$\partial_\zeta^2 x_\mathrm{c} + \omega_0^2 x_\mathrm{c} = \omega_0^2 x_\mathrm{b}. \tag{9}$$

If the beam meets the "short-pulse" limit $k_\beta x_\mathrm{b} \gg \omega_0\zeta$, the instability of the beam can be expressed by[53]

$$x_\mathrm{b}/x_{\mathrm{b}0} = 0.314A^{-3/2}\,\mathrm{e}^A \sin(k_\beta s - A/\sqrt{3} + \pi/4), \tag{10}$$

where $A = 1.3[(k_\beta s)(\omega_0\zeta)^2]^{1/3}$. Based on this theoretical model, we selected matching parameters between the beam and the plasma. Shortening the beam can reduce hosing instability and increase the number of oscillating electrons. As shown in Fig. 2, we compare the two cases $k_\mathrm{p}L_x = 5$ and $k_\mathrm{p}L_x = 13$ while keeping the plasma density $n_\mathrm{e} = 10^{18}$ cm$^{-3}$. The shorter beam can propagate 15 mm without significant hosing instability; while the longer beam, after propagating 5 mm, exhibits severe instability at the tail, significantly affecting the structure of the last bubble. Finally, the radiation brightness generated by the longer beam is generally an order of magnitude lower than that generated by the shorter beam. These results suggest that the beam length has an important effect on the stability and radiation characteristics of the system and provide a useful reference for further optimization of the experimental design.

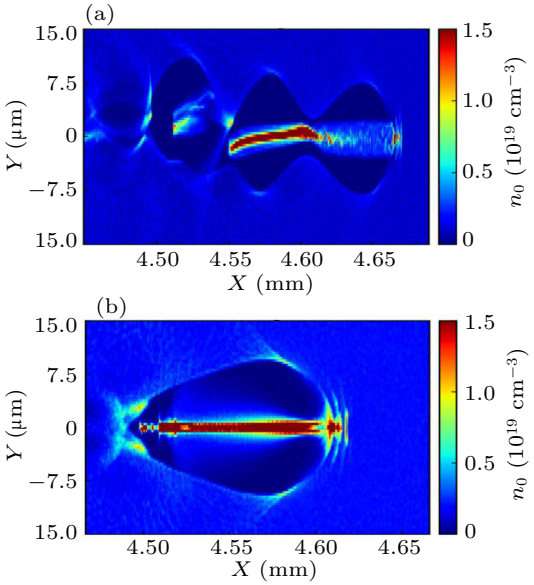



**Fig. 2.** The 3D-PIC simulation results of number density of the total electrons $n_0 = n_\mathrm{e} + n_\mathrm{b}$ for different beam longitudinal size (a) $k_\mathrm{p}L_x = 13$ and (b) $k_\mathrm{p}L_x = 5$ with the plasma density $n_\mathrm{e} = 1\times10^{19}$ cm$^{-3}$. At $t = 15$ ps, the longer beam exhibits significant hosing instability in the middle and rear sections, while the shorter beam remains stable at this time and is able to propagate over a long distance.

Considering the suboptimal quality of the drive beam, we investigated the evolution of the high-emittance drive beam based on the actual beam parameters in the experiment. In our simulations, at a plasma density of $1\times10^{19}$ cm$^{-3}$, we computed the electron and photon distributions for emittances of 3 mm·mrad and 50 mm·mrad, respectively. Because the transverse electric field of the scheme can reach about 10 GV/m, even if the electron divergence of the drive beam is large, the electron spectrum can remain basically unchanged, and the spot size remains small, as shown in Fig. 3. This result can be attributed to the transverse focusing force of the high-density plasma,[54] which effectively mitigates the poor characteristics of the initial drive beam. This result is consistent with the results in the experimental study.[55] In Eq. (1), $\boldsymbol{F}_\perp$ is a focusing and linear restoring force that drives the transverse oscillations of the electron across the cavity axis at the betatron frequency $\omega_\beta = \omega_\mathrm{p}/\sqrt{2\gamma}$. The plasma's focusing effect plays a crucial role in reducing the divergence of the electrons and maintaining a small-scale x-ray spot, which contributes to the high brightness of the observed radiation.

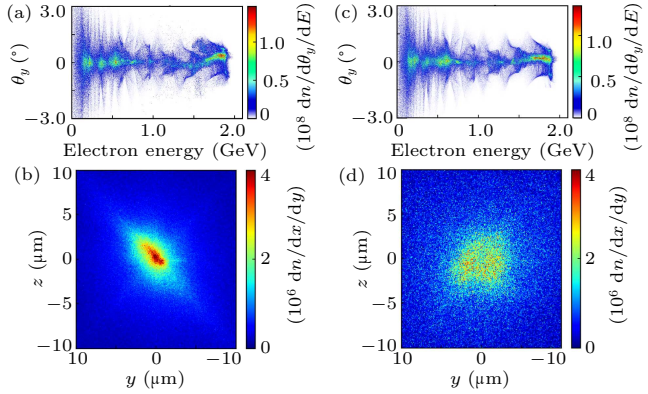



**Fig. 3.** The 3D-PIC simulation results of the spectral-angular distribution of the electrons and the spatial distribution of photons with different beam emittance (a), (b) $\varepsilon = 3$ mm·mrad and (c), (d) $\varepsilon = 50$ mm·mrad in the case of plasma density $n_\mathrm{e} = 1\times10^{19}$ cm$^{-3}$. In (a), (c), the angular distribution of the electron energy spectrum shows no significant change as the emittance increases. The peak energy of the electrons is 1.93 GeV, with a divergence angle of approximately $\pm3°$. Panels (b) and (d) illustrate that the spot size increases from 4.4 μm to 5.6 μm as the emittance grows.

As shown in Fig. 4, the increase in plasma density results in a higher radiation divergence due to the amplified interaction between the electron beam and the high-density plasma, leading to larger oscillations and wider emission angles of the electrons. Although the photon divergence increases with the density of the plasma, under matched beam parameters, the photon divergence remains at a relatively low level. Under these conditions, the betatron amplitude is around 10 μm, which is a relatively high amplitude that can be achieved over long distances. Furthermore, our findings revealed that adjusting plasma density allows direct manipulation of the emitted photon energy, with increased plasma density leading to higher

energy x-ray photons. This control adds significant flexibility and tunability to the x-ray radiation produced.

Based on the relationship between plasma density and emitted photon energy, we performed simulations with different $n_e$ and obtained the photon energy spectrum shown Fig. 4(e). By selecting the appropriate density ratio of plasma to beam, we demonstrated the ability to directly manipulate the energy range of emitted photons by controlling the plasma density. Specifically, as the plasma density increases, the energy of the x-ray photons also increases.

The physical basis for these findings lies in the interaction between plasma density and the dynamics of the electron radiation process. Since, in betatron, the radiation intensity parameter $K$ is usually less than 1, as shown in the Fig. 4(f), the radiated photon energy $\hbar\omega \propto \sqrt{n_e}$. The relationship between $\hbar\omega$ and $n_e$ satisfies theoretical equation (5). Detailed fitting curves, function slopes and regression coefficients are given in the supplementary material. The simulation results are slightly lower than the theory, because as the electron propagates in the plasma, the beam evolves over time, the electron energy spectrum widens and $\gamma$ changes (in supplementary material). This phenomenon underscores the pivotal role of plasma density in shaping the characteristics of the emitted x-ray radiation.

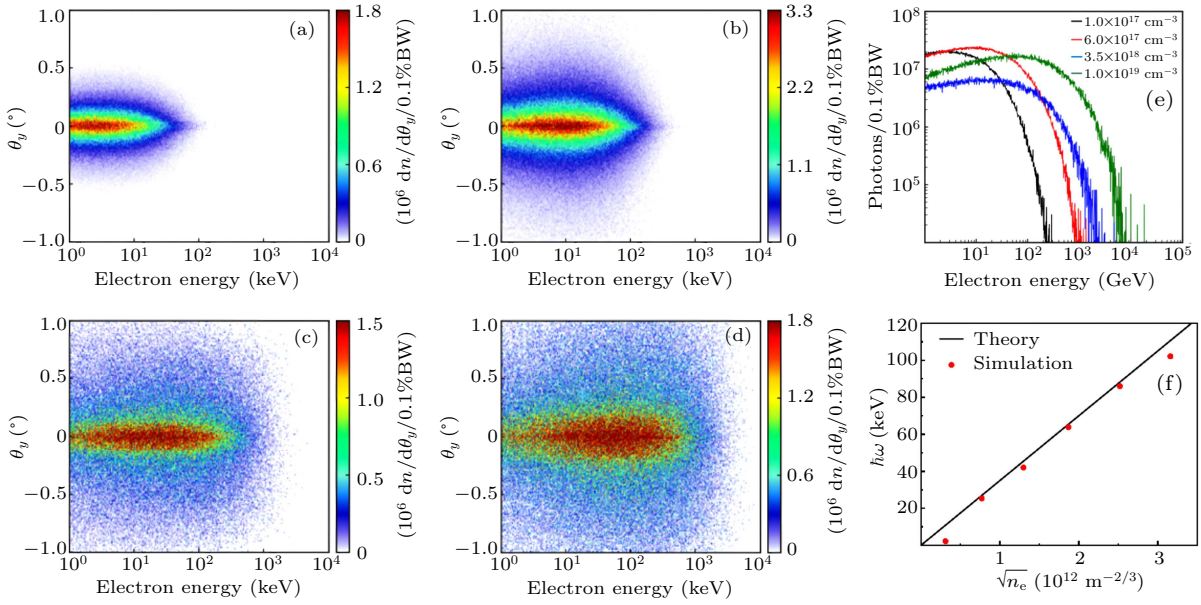



**Fig. 4.** The spectral-angular distribution of x-ray photons from the plasma of different densities: (a) $1 \times 10^{17}$ cm$^{-3}$, (b) $6 \times 10^{17}$ cm$^{-3}$, (c) $3.5 \times 10^{18}$ cm$^{-3}$ and (d) $1 \times 10^{19}$ cm$^{-3}$ in 3D-PIC simulations. (e) Comparison of photon energy spectra from different plasma densities. (f) Simulation results and theory of the relationship between $\hbar\omega$ and $\sqrt{n_e}$. As the plasma density increases, the photon energy and photon divergence also increase. The photon divergence angle (RMS) is 1.8 mrad in (a), 1.9 mrad in (b), 2.2 mrad in (c) and 2.3 mrad in (d). The center energy increases with the plasma density in the range of 2.2 keV to 102.1 keV, and the number of photons within 0.1%BW fluctuates around $10^7$.

In the situation depicted in Fig. 4, we were able to achieve tunable x-ray spectra while maintaining a high brightness of the radiation source. The radiation brightness and photon divergence under different plasma densities are shown in Table 1 and supplementary material. Here, the photon divergence angle $\theta_0$ for the first plasma density is 1.8 mrad and the photon divergence for the other cases is given as a ratio. Similarly, the x-ray peak brightness $B_0$ for the first plasma density is $4.8 \times 10^{22}$ photons/(0.1%BW·s·mm$^2$·mrad$^2$) and the brightness for the other cases is given as a ratio. These ratios are very close to 1, which shows that these sets of simulations maintain high x-ray quality while regulating photon energy. In addition, considering the more realistic situation in the experiment, we also simulated the situation of non-uniform plasma distribution. In hypergaussian plasma, the radiation quality and the trend of energy spectrum change are almost no different from that of uniform distribution (in supplementary material). This result proves the feasibility and effectiveness of our scheme and provides a useful reference for further optimization of experimental design.

**Table 1.** X-ray photon quality for beam-driven betatron radiation simulations.

| $n_e$ (cm$^{-3}$) | Center energy (keV) | $\theta_i/\theta_0$ | $B_i/B_0$ |
|---|---|---|---|
| $1.0 \times 10^{17}$ | 2.2 | 1.00 | 1.00 |
| $6.0 \times 10^{17}$ | 18.1 | 1.05 | 1.15 |
| $3.5 \times 10^{18}$ | 42.7 | 1.22 | 0.89 |
| $1.0 \times 10^{19}$ | 102.1 | 1.27 | 0.77 |

## 4. Conclusion

In conclusion, our research has demonstrated the successful realization of betatron x-ray sources with controllable spectra and presented a compact x-ray energy control scheme. Our approach involved the decomposition of the beam-driven betatron process into two distinct stages, namely, laser-driven electron acceleration and subsequent radiation generation arising from the oscillations of the accelerated electrons. Our focus was primarily on the latter stage, where we observed

that manipulation of the plasma density affords precise control over the central energy of the electron beam. Our endeavors have resulted in the achievement of tunable x-ray peak energies in the range from a few keV to several hundred keV, thereby expanding the controllable energy range by an order of magnitude. We studied the appropriate beam size and the ratio of the drive beam to plasma density, effectively utilizing the plasma's focusing effect to produce x-rays with low divergence, small spot size and high brightness even with a low-quality drive beam. At different central energies, the brightness of betatron radiation is in the range of $3.7 \times 10^{22}$ to $5.5 \times 10^{22}$ photons/(0.1%BW·s·mm$^2$·mrad$^2$) and the photon divergence angle is about 2 mrad. This tunable x-ray source is of great significance to a wide range of applications requiring photons of specific energy.

## Acknowledgements

Project supported by the National Natural Science Foundation of China (Grant Nos. 11921006 and 12175058), the Beijing Distinguished Young Scientist Program and National Grand Instrument Project (Grant No. SQ2019YFF01014400), and the Beijing Municipal Science & Technology Commission, Administrative Commission of Zhongguancun Science Park (Grant No. Z231100006023003). The PIC code EPOCH was in part funded by United Kingdom EPSRC (Grant Nos. EP/G054950/1, EP/G056803/1, EP/G055165/1, and EP/M022463/1).

## References

[1] Hogan M J, Barnes C D, Clayton C E, *et al.* 2005 *Phys. Rev. Lett.* **95** 054802
[2] Leemans W P, Nagler B, Gonsalves A J, Tóth C, Nakamura K, Geddes C G, Esarey E, Schroeder C B and Hooker S M 2006 *Nat. Phys.* **2** 696
[3] Strickland D and Mourou G 1985 *Opt. Commun.* **55** 447
[4] Tajima T and Dawson J M 1979 *Phys. Rev. Lett.* **43** 267
[5] Chen P, Dawson J M, Huff R W and Katsouleas T 1985 *Phys. Rev. Lett.* **54** 693
[6] Kiselev S, Pukhov A and Kostyukov I 2004 *Phys. Rev. Lett.* **93** 135004
[7] Pfeifer T, Spielmann C and Gerber G 2006 *Rep. Prog. Phys.* **69** 443
[8] Leemans W P, Gonsalves A J, Mao H S, Nakamura K, Benedetti C, Schroeder C B, Tóth C, Daniels J, Mittelberger D E, Bulanov S S, Vay J L, Geddes C G R and Esarey E 2014 *Phys. Rev. Lett.* **113** 245002
[9] Gonsalves A J, Nakamura K, Daniels J, *et al.* 2019 *Phys. Rev. Lett.* **122** 084801
[10] Liu J, Lu H, Lu H, *et al.* 2023 *Phys. Plasmas.* **30** 113103
[11] Zhao Y, Lehe R, Myers A, *et al.* 2020 *Phys. Plasmas.* **27** 113105
[12] Lundh O, Lim J, Rechatin C, *et al.* 2011 *Nat. Phys.* **7** 219
[13] Miller K G, Palastro J P, Shaw J L, *et al.* 2023 *Phys. Plasmas.* **30** 073902
[14] Kneip S, Nagel S R, Martins S F, *et al.* 2009 *Phys. Rev. Lett.* **103** 035002
[15] Wenz J, Schleede S, Khrennikov K, Bech M, Thibault P, Heigoldt M, Pfeiffer F and Karsch S 2015 *Nat. Commun.* **6** 7568
[16] Zhao C Z, Si S Y, Zhang H P, Xue L, Li Z L and Xiao T Q 2024 *Chin. Phys. B* **33** 014102
[17] Shao S, Li H, Yuan T, Sun X, Hua L, Liu Z and Sun T 2023 *Chin. Phys. B* **32** 080702
[18] Mahieu B, Jourdain N, Ta Phuoc K, Dorchies F, Goddet J P, Lifschitz A, Renaudin P and Cherbourg L 2018 *Nat. Commun.* **9** 3276
[19] Raimondi P, Benabderrahmane C, Berkvens P, *et al.* 2023 *Commun. Phys.* **6** 82
[20] Fuoss P H, Liang K S and Eisenberger P 1992 *Synchrotron Radiation Research* Vol. 1
[21] Pellegrini C, Marinelli A and Reiche S 2016 *Rev. Mod. Phys.* **88** 015006
[22] Zhang Y, Wang H W, Ma Y G, Liu L X, Cao X G, Fan G T, Zhang G Q and Fang D Q 2019 *Nucl. Sci. Tech.* **30** 87
[23] Albert F 2023 *Phys. Plasmas* **30** 050902
[24] Corde S, Phuoc K T, Fitour R, Faure J, Tafzi A, Goddet J P, Malka V and Rousse A 2011 *Phys. Rev. Lett.* **107** 255003
[25] Huang T, Robinson A, Zhou C, Qiao B, Liu B, Ruan S, He X and Norreys P 2016 *Phys. Rev. E* **93** 063203
[26] erri J, Davoine X, Kalmykov S Y and Lifschitz A 2016 *Phys. Rev. Accel. Beams* **19** 101301
[27] Balerna A and Mobilio S 2014 *Introduction to Synchrotron Radiation: Basics, Methods and Applications* (Springer) p. 3
[28] Leemans W, Gonsalves A, Mao H S, *et al.* 2014 *Phys. Rev. Lett.* **113** 245002
[29] Esarey E, Schroeder C B and Leemans W P 2009 *Rev. Mod. Phys.* **81** 1229
[30] Joshi C and Katsouleas T 2003 *Phys. Today* **56** 47
[31] Ferri J, Corde S, Döpp A, Lifschitz A, Doche A, Thaury C, Ta Phuoc K, Mahieu B, Andriyash A, Malka V and Davoine X 2018 *Phys. Rev. Lett.* **120** 254802
[32] Corde S, Ta Phuoc K, Lambert G, Fitour R, Malka V, Rousse A, Beck A and Lefebvre E 2013 *Rev. Mod. Phys.* **85** 1
[33] Rousse A, Phuoc K T, Shah R, Pukhov A, Lefebvre E, Malka V, Kiselev S, Burgy F, Rousseau J P, Umstadter D and Hulin D 2004 *Phys. Rev. Lett.* **93** 135005
[34] Albert F, Anderson S G, Gibson D J, Hagmann C A, Johnson M S, Messerly M, Semenov V, Shverdin M Y, Rusnak B, Tremaine A M, Hartemann F V, Siders C W, McNabb D P and Barty C P J 2010 *Phys. Rev. ST Accel. Beams* **13** 070704
[35] Xie B S, Wu H C, Wang H, Wang N Y and Yu M 2007 *Phys. Plasmas* **14** 073103
[36] Lu W, Huang C, Zhou M, Tzoufras M, Tsung F S, Mori W B and Katsouleas T 2006 *Phys. Plasmas* **13** 056709
[37] Lu W, Tzoufras M, Joshi C, Tsung F S, Mori W B, Vieira J, Fonseca R A and Silva L O 2007 *Phys. Rev. ST Accel. Beams* **10** 061301
[38] Esarey E, Shadwick B A, Catravas P and Leemans W P 2002 *Phys. Rev. E* **65** 056505
[39] Kostyukov I, Kiselev S and Pukhov A 2003 *Phys. Plasmas* **10** 4818
[40] Phuoc K T, Burgy F, Rousseau J P, Malka V, Rousse A, Shah R, Umstadter D, Pukhov A and Kiselev S 2005 *Phys. Plasmas* **12** 023101
[41] Pukhov A, Gordienko S, Kiselev S and Kostyukov I 2004 *Plasma Phys. Control. Fusion* **46** B179
[42] Chen P, Su J J, Dawson J M, Bane KL F and Wilson P B 1986 *Phys. Rev. Lett.* **56** 1252
[43] Ferri J, Davoine X, Kalmykov S and Lifschitz A 2016 *Phys. Rev. Accel. Beams* **19** 101301
[44] Arber T, Bennett K, Brady C, *et al.* 2015 *Plasma Phys. Control. Fusion* **57** 113001
[45] Teixeira F L, Sarris C, Zhang Y, *et al.* 2023 *Nat. Rev. Methods Primers* **3** 75
[46] Litos M, Adli E, An W, *et al.* 2014 *Nature* **515** 92
[47] Esarey E, Schroeder C B and Leemans W P 2009 *Rev. Mod. Phys.* **81** 1229
[48] Liang L, Xia G, Saberi H, Farmer J P and Pukhov A 2022 arXiv preprint arXiv:2204.13199
[49] Lu W, Huang C, Zhou M, Mori W and Katsouleas T 2005 *Phys. Plasmas* 12
[50] Heine R 2021 *Phys. Rev. Accel. Beams* **24** 011602
[51] Baistrukov M and Lotov K 2022 *Plasma Phys. Control. Fusion* **64** 075003
[52] Rosenzweig J B, Breizman B, Katsouleas T and Su J 1991 *Phys. Rev. A* **44** R6189
[53] Huang C, Lu W, Zhou M,*et al.* 2007 *Phys. Rev. Lett.* **99** 255001
[54] San Miguel Claveria P, Adli E, *et al.* 2019 *Phil. Trans. Roy. Soc. A* **377** 20180173
[55] Bjorklund Svensson J, Guenot D, Ferri J, Ekerfelt H, Gallardo Gonzalez I, Persson A, Svendsen K, Veisz L and Lundh O 2021 *Nat. Phys.* **17** 639